10.1109/ULTSYM.2015.0197

Simulation Studies of Filtered Spatial Compounding (FSC) and Filtered Frequency Compounding (FFC) in Synthetic Transmit Aperture (STA) Imaging

Ping Gong, Michael C. Kolios, Yuan Xu
Physics Department
Ryerson University
Toronto, Canada
yxu@ryerson.ca

***Abstract*—Speckle patterns are formed by constructive and destructive interference of backscattered waves from non-resolvable scatterers. Speckles can result in a low speckle signal-to-noise ratio (*s*SNR) in the ultrasound images of even a uniform sample. Speckles also reduce the contrast-to-noise-ratio (CNR) and the detectability of lesions, especially for low contrast lesions. Moreover, undesired signals arising from off-axis targets can result in sidelobes and clutters which lead to even lower lesion CNR. Typically, the speckle SNR can be increased by compounding, either spatial compounding (SC) or frequency compounding (FC). Here we propose methods to implement a 2-dimentional (2-D) aperture domain filter in the SC and FC processes, which are referred to as filtered spatial compounding (FSC) and filtered frequency compounding (FFC), for synthetic transmit aperture (STA) imaging. Both FSC and FFC can provide more homogeneous speckle patterns with improved speckle SNR and lesion CNR. The aperture domain filter reduces the interference effect of the off-axis signals to further enhance lesion CNR. Consequently, the target detectabilities (lesion-signal-to-noise ratio (*l*SNR)) in both FSC and FFC are increased significantly, up to around 3 times, compared to that in the standard delay-and-sum (DAS) method.**

Keywords— Spatial compounding, frequency compounding, 2-D aperture domain filter, speckle suppression

I. INTRODUCTION

Speckles are formed by constructive and destructive interference of scattered waves from a cluster of non-resolvable scatterers [1]. They usually limit the speckle signal-to-noise ratio (*s*SNR), reduce the image contrast-to-noise-ratio (CNR) and detectability of the targets, especially for low CNR targets. The image CNR can be further degraded by undesired signals arising from off-axis targets such as sidelobes and clutters.

Typically, speckle SNR can be improved by either spatial compounding (SC) [1-3] or frequency compounding (FC) [4-6]. Spatial compounding (SC) can be achieved by using different beam orientations or laterally translated sub-apertures to acquire sub-images. Afterwards, the sub-images are added incoherently to perform compounding [7]. In FC, sub-images can be obtained by either varying the central frequency of the transmitted pulse or by dividing the signal spectrum into a bank of narrow sub-bands [7]. Both SC and FC techniques can provide images with more homogeneous speckle patterns and improved image CNR but they are at the expense of temporal or spatial resolutions.

Various approaches have been proposed to overcome the disadvantages in either SC or FC. The temporal resolution loss in SC, which is due to the involvement of multiple scans, can be compensated by recursive imaging [8], or accomplishing compounding on partially overlapping receive sub-apertures rather than on transmit [9], or using the new system for SC imaging as introduced by Behar et al [10]. Spatial compounding has also been implemented in synthetic transmit aperture (STA) imaging [8, 11, 12] which allows the beam to be steered to any angle without temporal resolution loss. The axial resolution loss in the FC technique, which is caused by the narrow bandwidth of each sub-band, can be reduced by using the resolution enhancement compression (REC) technique [13] or 2-D directive filters [14-16] to provide effectively the same bandwidth as the original image.

Here we propose methods to implement a 2-dimentional (2-D) aperture domain filter prior to both spatial and frequency compounding processes, which are referred to as filtered spatial compounding (FSC) and filtered frequency compounding (FFC), on synthetic transmit aperture (STA) imaging data [17]. Both compounding effects provide ultrasound images with enhanced speckle SNR and image CNR. The 2-D aperture domain filter suppresses the off-axis signals so that it further improves the image CNR. Neither FSC nor FFC introduces any additional transmission events so that the same frame rate is preserved as in the traditional delay-and-sum (DAS) beamforming. The spatial resolution in FSC is retained as in DAS, leading to significantly improved target detectability (lesion signal-to-noise ratio (*l*SNR)). The axial resolution in FFC image is degraded as in some other frequency compounding methods. Despite the degradation of resolution, the CNR improvement in FFC results in a greatly enhanced target detectability in the FFC images due to the combination of spatial compounding and frequency compounding.

In section II, the theory of the FSC and FFC techniques are explained and then the implementation of these two techniques

are described. The quantification parameters for image quality are introduced as well. In section III, the results using both simulated techniques are shown and the image qualities are assessed and compared with images reconstructed by the standard delay-and-sum (DAS) and the conventional spatial compounding (CSC). In section IV, the performance for both FSC and FFC is discussed and the conclusion is drawn.

II. METHODS

A. Theory

The received channel RF signals in STA imaging method can be presented as a 3-D data matrix (i.e. time × receive × transmit). First, various focusing delays caused by time-of-flight differences are compensated to each receive channel ($\mathbf{R}$) under the transmission of each element ($\mathbf{T}$) to focus at one image pixel. After the RF signals are aligned along the time direction, they can be added up coherently across both $\mathbf{T}$ and $\mathbf{R}$ directions to produce the value of the corresponding image point as in the conventional DAS. In STA imaging, after the coherent summation along $\mathbf{R}$ dimension, the signals can also be combined incoherently along $\mathbf{T}$ dimension as in the CSC, which can be treated as using a translated transmit sub-aperture for compounding. In FSC or FFC, before the summation along either $\mathbf{T}$ or $\mathbf{R}$, we implement a 2-D aperture domain filter to the aligned RF data along both $\mathbf{T}$ and $\mathbf{R}$ directions to reduce the off-axis signals which have high spatial frequencies in the aperture-time domain

$$\mathbf{P}_{\text{filtered}} = \mathbf{HP} \tag{1}$$

where $\mathbf{P}$ is the 2-D Fourier transform of the 3-D STA data matrix over the $\mathbf{T}$ and $\mathbf{R}$ directions; $\mathbf{H}$ is the 2-D aperture domain filter as,

$$\mathbf{H} = H_n \times H_m \tag{2}$$

The aperture domain filter $\mathbf{H}$ is designed as a low-pass filter along both the transmit (H_m) and receive (H_n) directions. The Hanning window function is used to design the low-pass filters. Afterwards, spatial compounding (SC) is applied to the filtered aligned RF data in the FSC via *incoherent summation* to suppress speckles and therefore, to improve the image CNR and *l*SNR,

$$I_{\text{FSC}}(x,z) = \sum_{m=1}^{M}\left\{\sum_{n=1}^{N}\text{ENV}\left[p_{\text{filtered}}(t-\Delta t_{nm},n,m)\right]\right\} \tag{3}$$

where $p_{\text{filtered}}(t-\Delta t_{nm},n,m)$ is the inverse Fourier transform of $\mathbf{P}_{\text{filtered}}$, which is the filtered STA RF signal received by the element $n(n=1:N)$ and transmitted by the element $m(m=1:M)$ with a focusing delay Δt_{nm}. ENV represents the envelop detection by Hilbert transform. $I_{\text{FSC}}(x,z)$ denotes the reconstructed image point with the coordinate of (x,z) in the FSC technique.

In FFC, the corresponding image value can be reconstructed using

$$I_{\text{FFC}}(x,z) = \sum_{m=1}^{M}\sum_{n=1}^{N}\sum_{f=f_{\text{low}}}^{f_{\text{high}}}\left|P_{\text{filtered}}(f,k_n,k_m)\right|^2 \tag{4}$$

where $P_{\text{filtered}}(f,k_n,k_m)$ is the 3-D Fourier transform of $p_{\text{filtered}}(t-\Delta t_{nm},n,m)$. The amplitude of the frequency components which are outside the pass-band range of (f_{low} - f_{high}) are zero (2-8 MHz with central frequency at 5 MHz was used in this paper).

B. Simulation Configuration

The proposed FSC and FFC methods were tested with Field II simulations [18, 19]. A 64-element, 2-cm-wide, 5 MHz linear array was placed 15 mm above a 1 cm × 2 cm (lateral × axial) tissue mimicking phantom which contained two 4-mm-diameter inclusions (left: hyper, right: hypo echoic) and a point inclusion at the center. Standard STA RF data were acquired from the phantom. The hyper- and hypo-inclusions, which were barely visible in the standard DAS image, had a scattering strength of 1.7 and 0.6 times of that in the background, respectively. The same RF data were processed by DAS, CSC, FSC, and FFC methods. Then all the beamformed signals were displayed as log-enveloped images.

C. Quantification Metrics

In this paper, the speckle SNR which measures the speckle fluctuation of the background was characterized using [8].

$$s\text{SNR} = \mu_{\text{background}} / \sigma_{\text{background}} \tag{5}$$

where $\mu_{\text{background}}$ and $\sigma_{\text{background}}$ denote the mean and the standard deviation of the envelope detected speckles in the background, respectively.

Image CNR for both the hyper and hypo inclusions were defined as [20].

$$\text{CNR} = \frac{\left\langle S_{\text{ROI}}\right\rangle - \left\langle S_{\text{background}}\right\rangle}{\sqrt{\sigma_{\text{ROI}}^{\,2} + \sigma_{\text{background}}^{\,2}}} \tag{6}$$

where $\left\langle S_{\text{ROI}}\right\rangle$ and $\left\langle S_{\text{background}}\right\rangle$ denote the mean values of log-enveloped region of interest (ROI) and background at the same depth, respectively. σ_{ROI} and $\sigma_{\text{background}}$ are the standard deviation in the ROI and background, respectively.

*l*SNR determines the detectability of an isolated target from the background. It is related to both the lesion CNR and the spatial resolution [13, 21, 22] and is calculated as

$$l\text{SNR} = \frac{\left|\text{CNR}\right|\cdot d}{\sqrt{\text{FWHM}_{\text{lat}}\cdot\text{FWHM}_{\text{axial}}}} \tag{7}$$

where d is the diameter of the target and FWHM stands for full width at half maximum.

III. RESULTS

Fig. 1 shows the log-enveloped images reconstructed using DAS (a), CSC (b), FSC (c), and FFC (d), respectively. The 2-D aperture domain filters used in FSC and FFC were two Hanning window functions with the cut-off frequencies (the frequency where the amplitude decreased to zero) at 1.0 cm^{-1} and 2.6 cm^{-1}, respectively. These values were selected by trial and error in order to provide optimized image quality in each technique.

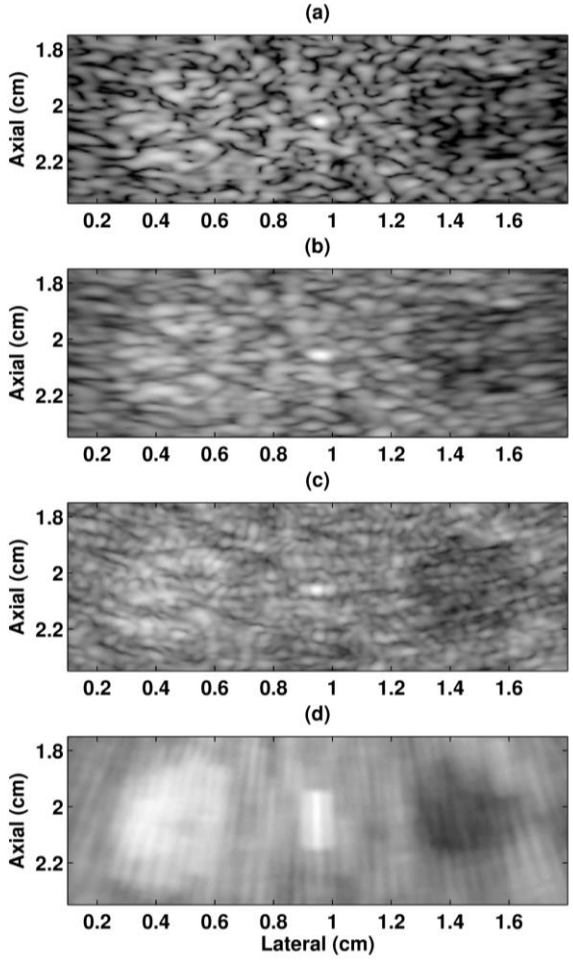

Fig. 1. Beamformed images of a simulated tissue mimicking phantom reconstructed with (a) DAS, (b) CSC (c) FSC, and (d) FFC, respectively. The image dynamic range is 35 dB

Fig. 2 displays the lateral line plots across the point target at the center from the images reconstructed using the above four techniques (DAS, CSC, FSC, and FFC). Detailed comparison is shown in TABLE I in terms of the background speckle SNR, lateral and spatial resolutions [as assessed by the FWHM of the point spread function (PSF)], the lesion CNR, and the target detectability (as assessed on both the hyper and hypo inclusions). The percentage values shown in brackets present the improvement ('+') and degradation ('-') of different quality metrics relative to the values in the DAS images.

FSC and FFC (Fig. 1 (c) and (d)) provided images with more homogeneous speckle patterns and significantly improved *s*SNR values (especially in FFC image). The FSC image offered improved lateral resolution (Fig. 1 and 2) and CNR values for both hyper and hypo inclusions, leading to a significant enhancement in target detectability. The FFC method sacrificed image resolution due to the frequency compounding. However, the method combined SC with FC, resulting in a better target detectability (*l*SNR values) than the FSC technique alone.

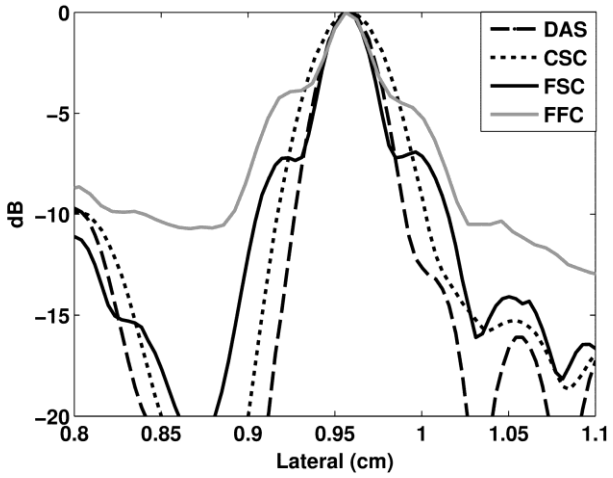

Fig. 2. Lateral line plots through the point target in the center of the images in DAS (dashed line), CSC (dotted line), FSC (solid black line), and FFC (solid gray line).

TABLE I. Quantification of *s*SNR, resolutions, CNR and *l*SNR values of the simulated tissue mimicking phantom images (Fig. 1) obtained by (a) DAS, (b) CSC, (c) FSC, and (d) FFC, respectively. The percentage values shown in brackets present the improvement ('+') and degradation ('-') of different quality metrics measured in CSC, FSC and FFC images relative to the values in the DAS images.

Technique	DAS	CSC		FSC		FFC	
***s*SNR**	1.78	2.41	(+35%)	2.65	(+49%)	6.39	(+259%)
$FWHM_{lat}$ [mm]	0.46	0.65	(-41%)	0.42	(+9%)	0.96	(-109%)
$FWHM_{axial}$ [mm]	0.30	0.30	(+0%)	0.30	(+0%)	2.08	(-593%)
CNR (hyper)	0.69	0.93	(+35%)	0.69	(+0%)	3.18	(+361%)
CNR (hypo)	-0.32	-0.44	(+38%)	-1.21	(+278%)	-5.09	(+1491%)
***l*SNR (hyper)**	7.43	8.42	(+13%)	7.78	(+5%)	9.00	(+21%)
***l*SNR (hypo)**	3.45	3.99	(+16%)	13.6	(+294%)	14.41	(+318%)

IV. Discussion and Conclusion

In the FSC method, considering the convolution property of the Fourier transform, multiplying the 2-D aperture domain filter (**H**) with the **T/R** aperture RF data (**P**) in the spatio-frequency domain as in (1) is equivalent to a sub-aperture compounding applied to both the **T** and **R** domains (i.e. the inverse Fourier transform of the filter **H** is h , which corresponds to the sub-aperture that convolves with the **T/R** aperture data (p) in the aperture domain).

Improved lateral resolution can be observed from the simulated FSC images because of the removal of the dynamic apodization as used in DAS and CSC. Consequently, the active sub-aperture used for FSC with a 1.0 cm^{-1} cut-off frequency of the Hanning window almost covered the entire array rather than just part of the transducer array as in DAS. The CNR was enhanced as a compounding effect, which also contributed to the improvement in the target detectability.

FFC is a combination of both SC and FC methods as it is equivalent to the compounding of many sub-images, each of which is reconstructed from a sub-aperture and a sub-band of the complete STA data. Consequently, the CNR values in FFC images were better than the FSC images

The target detectability (*l*SNR) improvement of the hypo inclusion was greater than the hyper one (TABLE I). This is due to the fact that the hypo inclusion was more sensitive to the sidelobe effects and therefore, suffered more from interference as in DAS and CSC techniques. The strong suppression of sidelobes by the 2-D aperture domain filter, results in a larger enhancement of the detection of the hypoechoic lesions in both FSC and FFC images.

In conclusion, filtered spatial compounding (FSC) and frequency compounding (FFC) reconstruction techniques have been proposed in this paper for synthetic transmit aperture imaging using a 2-D aperture domain filter. Simulation studies on both techniques demonstrated improved image qualities in terms of lateral resolution (for FSC), image CNR, and target detectability.

V. Acknowledgement

We would like to thank our funding agencies: the Natural Sciences and Engineering Research Council of Canada (NSERC), the Canada Foundation for Innovation (CFI) and Ryerson University. We are grateful to Dr. Richard Cobbold, Dr. Jahan Tavakkoli, Ying Li and Dea Young for their valuable discussion and suggestions.

References

[1] C. B. Burckhardt, "SPECKLE IN ULTRASOUND B-MODE SCANS," *IEEE Transactions on Sonics and Ultrasonics*, vol. 25, pp. 1-6, 1978.

[2] D. P. Shattuck and O. T. Vonramm, "COMPOUND SCANNING WITH A PHASED-ARRAY," *Ultrasonic Imaging*, vol. 4, pp. 93-107, 1982.

[3] M. O'Donnell and S. D. Silverstein, "Optimum displacement for compound image generation in medical ultrasound," *IEEE transactions on ultrasonics, ferroelectrics, and frequency control*, vol. 35, p. 470, 1988.

[4] H. E. Melton and P. A. Magnin, "A-MODE SPECKLE REDUCTION WITH COMPOUND FREQUENCIES AND COMPOUND BANDWIDTHS," *Ultrasonic Imaging*, vol. 6, pp. 159-173, 1984.

[5] G. E. Trahey, J. W. Allison, S. W. Smith, and O. T. Vonramm, "A QUANTITATIVE APPROACH TO SPECKLE REDUCTION VIA FREQUENCY COMPOUNDING," *Ultrasonic Imaging*, vol. 8, pp. 151-164, Jul 1986.

[6] S. M. Gehlbach and F. G. Sommer, "Frequency Diversity Speckle Processing," *Ultrasonic Imaging*, vol. 9, pp. 92-105, Apr 1987.

[7] J. Park, J. B. Kang, 장진호, and 유양모, "Speckle Reduction Techniques in Medical Ultrasound Imaging," *Biomedical Engineering Letters (BMEL)*, vol. 4, pp. 32-40, 2014.

[8] J. M. Hansen and J. A. Jensen, "Compounding in Synthetic Aperture Imaging," *IEEE Transactions on Ultrasonics Ferroelectrics and Frequency Control*, vol. 59, pp. 2054-2065, Sep 2012.

[9] K. F. M. V. Ustuner, CA), Bradley, Charles E. (Burlingame, CA), Need, Daniel E. (Mountain View, CA), "Medical ultrasonic imaging method and system for spatial compounding," United States Patent 6527720, 2003.

[10] V. Behar, D. Adam, and Z. Friedman, "A new method of spatial compounding imaging," *Ultrasonics*, vol. 41, pp. 377-384, Jul 2003.

[11] J. M. Hansen and J. A. Jensen, "Performance of synthetic aperture compounding for in-invo imaging," in *Ultrasonics Symposium (IUS), 2011 IEEE International*, 2011, p. 1148.

[12] J. M. Hansen, and J. A. Jensen, "Optimizing Synthetic Aperture Compound Imaging," *2012 IEEE International Ultrasonics Symposium (Ius)*, pp. 382-385, 2012.

[13] J. R. Sanchez and M. L. Oelze, "An ultrasonic imaging speckle-suppression and contrast-enhancement technique by means of frequency compounding and coded excitation," *IEEE Trans Ultrason Ferroelectr Freq Control*, vol. 56, pp. 1327-39, Jul 2009.

[14] R. G. Dantas and E. T. Costa, "Ultrasound speckle reduction using modified Gabor filters," *IEEE Transactions on Ultrasonics Ferroelectrics and Frequency Control*, vol. 54, pp. 530-538, Mar 2007.

[15] P. Liu and D. Liu, "Directive Filtering Schemes for Frequency Compounding in Ultrasound Speckle Reduction," *Proceedings of 2008 International Pre-Olympic Congress on Computer Science, Vol Ii: Information Science and Engineering*, pp. 13-17, 2008.

[16] P. Liu, and D. Liu "Oriented Demodulation and Frequency Splitting for Directive Filtering Based Compounding," *2008 IEEE Ultrasonics Symposium, Vols 1-4 and Appendix*, pp. 353-356, 2008.

[17] J. A. Jensen, S. I. Nikolov, K. L. Gammelmark, and M. H. Pedersen, "Synthetic aperture ultrasound imaging," *Ultrasonics*, vol. 44, Supplement, p. e5, 12/22 2006.

[18] J. A. Jensen and N. B. Svendsen, "Calculation of pressure fields from arbitrarily shaped, apodized, and excited ultrasound transducers," *Ultrasonics, Ferroelectrics and Frequency Control, IEEE Transactions on*, vol. 39, p. 262, 1992.

[19] J. A. Jensen, "Field: A program for simulating ultrasound systems," *Med. Biol. Eng. Comput.*, vol. 34, pp. 351-353, 1996.

[20] K. F. Üstüner and G. L. Holley, "Ultrasound Imaging System Performance Assessment," Siemens Medical Solutions USA, Inc2003.

[21] S. W. Smith, R. F. Wagner, J. M. Sandrik, and H. Lopez, "LOW CONTRAST DETECTABILITY AND CONTRAST DETAIL ANALYSIS IN MEDICAL ULTRASOUND," *Ultrasonic Imaging*, vol. 4, pp. 188-188, 1982.

[22] M. F. Insana and T. J. Hall, "Visual detection efficiency in ultrasonic imaging: A framework for objective assessment of image quality," *The Journal of the Acoustical Society of America*, vol. 95, pp. 2081-2090, 1994.